JOURNAL OF CATALYSIS 130, 374–391 (1991)

Effect of Catalyst Structure and Carbon Deposition on Heptane Oxidation over Supported Platinum and Palladium

ANDREW B. KOOH, WHA-JIN HAN, RAYMOND G. LEE, AND ROBERT F. HICKS[1]

UCLA Chemical Engineering Department, 5531 Boelter Hall, Los Angeles, California 90024-1592

Received November 7, 1989; revised March 6, 1991

A series of supported platinum and palladium catalysts were tested for heptane oxidation at 75 to 200°C, 20 Torr heptane, 245 Torr oxygen, 795 Torr helium, and conversions below 1%. At these low temperatures, carbon fouls the metal surface. The decline in the turnover frequency with time is accurately fitted with this function: $TOF_{obs} = TOF_A\exp(-k_At) + TOF_b\exp(-k_Bt)$. The turnover frequencies of the *A* and *B* sites depend on catalyst structure. At 140°C, the activities of the *A* sites are: 0.02 s^{-1} for <20 Å platinum crystallites, 0.45 s^{-1} for >50 Å platinum crystallites, 0.002 s^{-1} for <20 Å palladium crystallites, and 0.07 s^{-1} for >50 Å palladium crystallites. The activity of the *B* sites is 10 times higher on platinum compared to palladium, and is 4 times higher on large crystallites compared to small ones. The amount of carbon on the catalyst depends on the half power of reaction time. These and other results indicate that carbon formed on the metal diffuses slowly to the support. The coke formation and the deactivation rate are much lower on <20 Å metal crystallites compared to >50 Å metal crystallites. On large metal crystallites, the coke formation rate per exposed metal atom and the deactivation rate depend on the number of metal particles on the support and the support composition. Decreasing the number of particles sixfold increases the carbon deposition rate by 2.5 times, and decreases the deactivation rate by 5.3 times. Switching from zirconia (40 m^2/g) to alumina (83 m^2/g) at 5.0 wt% platinum increases the carbon deposition rate 5 times, and decreases the deactivation rate 5.5 times. Evidently, the faster the carbon migrates from the metal to the support, the slower the carbon fouls the metal surface. © 1991 Academic Press, Inc.

INTRODUCTION

Precious metal catalysts are used extensively to reduce hydrocarbon emissions from automobiles (*1, 2*) and industrial processes (*3*). Since smog in Southern California and in other urban regions of the United States is worsening, greater demands will be placed on the catalyst to oxidize all the hydrocarbons. For example, in California, the emission standard for reactive organic gases has been lowered from 0.41 to 0.25 g/mile, effective January 1991 (*4*). In addition, new gasoline formulations have been introduced which produce less carbon monoxide and nitrogen oxide, but the same or higher levels of hydrocarbons. Hydrocarbon oxidation over precious metals has not been studied nearly as much as carbon monoxide oxidation and nitrogen oxide reduction. Clearly, there is a need to develop a fundamental understanding of this catalytic reaction.

Several studies have been published on the oxidation of methane (*5–15*), C_2–C_7 alkanes (*10, 15–20*), olefins (*17, 21–30*), and aromatics (*20, 28*) over precious metals. It has been found that methane is the most difficult hydrocarbon to oxidize (*4, 10, 15*). We have shown that the rate of methane oxidation depends on catalyst composition and structure (*13, 14*). Palladium is more active than platinum, and large metal crystallites are more active than small metal crystallites. The rate of C_2–C_7 alkane oxidation also has been shown to depend on catalyst composition and structure (*10, 15, 17, 19*). Platinum is more active than palladium, and large crystallites are more active than small ones. However, the magnitude of

[1] To whom correspondence should be addressed.

0021-9517/91 $3.00
Copyright © 1991 by Academic Press, Inc.
All rights of reproduction in any form reserved.

these effects is uncertain. In the alkane oxidation studies which examined the effect of particle size, the reaction rates were measured at high conversions where heat and mass transfer may have influenced the results. Also, the deactivation of the catalyst during the run was not considered.

In this work, we have investigated the effects of catalyst composition and structure on the intrinsic rate of heptane oxidation over supported platinum and palladium. Seven platinum catalysts and four palladium catalysts were prepared with dispersions ranging from 3 to 81%. Reaction rates were measured as a function of time at low conversion under a standard set of conditions. After reaction, the catalysts were characterized by *in situ* gas titration, temperature-programmed oxidation, and infrared spectroscopy of adsorbed carbon monoxide. We found that the catalyst activity falls rapidly with time because carbon fouls the metal surface. The effects of metal composition, support composition, and metal particle size on the rate of heptane oxidation and the rate of deactivation are described below.

EXPERIMENTAL

Materials

The catalyst supports were Degussa, flame-synthesized aluminum oxide "C," and zirconium oxide. The alumina was calcined in air at 1000°C for 24 h, while the zirconia was calcined in air at 600°C for 24 h. After the treatments, the alumina and zirconia surface areas were 83 and 40 m^2/g, respectively. Various amounts of platinum and palladium were deposited on the supports from $Pt(NH_3)_4Cl_2$, H_2PtCl_6, and H_2PdCl_4. On sample number 1, the platinum was deposited by ion exchange at 25°C. On all the other samples, the platinum and palladium were deposited by incipient wetness impregnation. All the samples were dried at 125°C for 2 h, then calcined in air at temperatures between 500 and 900°C for 2 h. Following oxidation, the metal loadings were measured by inductively coupled plasma emission spectroscopy. Table 1 lists the method of preparation, the metal weight loading and the initial dispersion of each catalyst.

TABLE 1

Preparation of the Catalysts

Sample number	Support	Metal salt	Calcined 2 h in air at (°C)	Metal loading (%)	Initial dispersion (%)
1	ZrO_2	$Pt(NH_3)_4Cl_2$	500	0.4	81
2	ZrO_2	$Pt(NH_3)_4Cl_2$	500	0.3	56
3	ZrO_2	$Pt(NH_3)_4Cl_2$	500	5.0	19
4	Al_2O_3	$Pt(NH_3)_4Cl_2$	500	0.3	58
5	Al_2O_3	H_2PtCl_6	600	0.8	13
6	Al_2O_3	H_2PtCl_6	700	0.8	6
7	Al_2O_3	H_2PtCl_6	600	5.0	10
8	Al_2O_3	H_2PdCl_4	700	0.2	81
9	Al_2O_3	H_2PdCl_4	900	0.2	55
10	Al_2O_3	H_2PdCl_4	700	2.3	10
11	Al_2O_3	H_2PdCl_4	900	2.3	3

The gases used for catalyst treatment, reaction and chemisorption were Liquid Air Corp. helium (99.995%), hydrogen (99.995%), and oxygen (99.995%) and Matheson research purity carbon monoxide (99.99%). The heptane, OmniSolv from EM Science, was 99.9% pure and contained less than 0.25 ppb sulfur. The gases were purified further by passing them through 13X molecular sieve traps held at −78°C. The hydrogen and helium were also passed through Alltech oxygen adsorbent.

Methods

The initial metal dispersion of each sample was determined by hydrogen and carbon monoxide adsorption (*31*). From 1 to 3 g of sample was placed in a glass tube and attached to the adsorption apparatus. Then the sample was reduced in hydrogen at 300°C for 1 h, evacuated to 1×10^{-6} Torr (1 Torr = 133 N/m^2) at 300°C for 0.5 h, and cooled in vacuum to 25°C. The catalyst was dosed periodically with gas and the amount adsorbed recorded as a function of pressure. The gas uptake was determined by extrapolating the linear portion of the isotherm at saturation coverage back to zero pressure. The dispersions of the platinum catalysts

were determined by hydrogen titration of preadsorbed oxygen, assuming 1.5 H_2 adsorbed per PtO_s (*32*). The dispersions of the palladium catalysts were determined by carbon monoxide adsorption, assuming 1.0 CO adsorbed per Pd_s (*33*).

The rate of heptane oxidation was determined in a fixed-bed microreactor. Between 0.1 and 0.7 g of catalyst pellets (32–60 mesh) were loaded into a 4-mm-i.d. glass tube. A thermocouple was mounted just upstream of the bed, and the tube was placed in a furnace. The reaction products were analyzed by on-line gas chromatography, using an HP 5890A gas chromatograph equipped with HaySep Q and 13X molecular sieve columns and a thermal conductivity detector. Carbon dioxide was the only product observed. Throughout the experiments, the carbon dioxide concentration ranged between 600 and 25 ppm. The lowest concentrations of carbon dioxide and carbon monoxide detectable were 10 ppm.

The procedure for evaluating the catalysts was as follows. The sample was heated in 50 cm^3/min oxygen at 11°C/min to 500°C, oxidized at 500°C for 20 min, cooled to 300°C, purged in 50 cm^3/min helium for 10 min, and reduced in 50 cm^3/min hydrogen at 300°C for 20 min. This cycle of oxidation and reduction was repeated twice more to remove as much carbon as possible from the catalyst surface. Further cycles did not change the baseline quantity of carbon on the catalyst. The sample was next cooled in helium to 25°C, reheated in 22 cm^3/min oxygen and 120 cm^3/min helium at 11°C/min to 500°C, oxidized at 500°C for 20 min, cooled to 300°C, purged in 50 cm^3/min helium for 10 min, reduced in 50 cm^3/min hydrogen at 300°C for 20 min, and cooled in 50 cm^3/min helium to 60°C. During temperature-programmed heating in oxygen, the amount of carbon converted to carbon dioxide was monitored with the gas chromatograph. The baseline quantity of carbon was calculated by integrating under the curve of the rate of CO_2 production versus time. Once the sample had cooled to 60°C, the helium flow was reduced to 20 cm^3/min and the valving to the gas chromatograph was switched to the pulse adsorption mode. The catalyst was consecutively dosed with oxygen, hydrogen, carbon monoxide, and oxygen. From the number of hydrogen, carbon monoxide, and oxygen pulses adsorbed, the dispersion was calculated, assuming 3/2 H_2, 1 CO, and 1 O_2 adsorbed per exposed metal atom. Next, the sampled was reduced in 50 cm^3/min hydrogen at 300°C for 20 min and cooled in helium to the reaction temperature. Heptane oxidation was begun by introducing 20 Torr heptane, 245 Torr oxygen, and 795 Torr helium at 235 cm^3/min. This mixture contained an 11% stoichiometric excess of oxygen. The reaction was allowed to proceed for 2 to 16 h. The amount of catalyst and the reaction temperature were chosen to keep the heptane conversion below 1%, thereby ensuring no effect of heat or mass transfer on the rate.

Periodically throughout a run the reaction was stopped by switching to 30 cm^3/min helium, and either the dispersion measured by pulse adsorption, or the surface carbon analyzed by temperature-programmed oxidation. The metal dispersion was normally measured by consecutively titrating the catalyst with hydrogen, oxygen, hydrogen, carbon monoxide, and oxygen at 60°C. In some instances, an alternative sequence was used consisting of carbon monoxide, oxygen, hydrogen, carbon monoxide, and oxygen at 60°C. The temperature-programmed oxidation was carried out by heating the sample in 22 cm^3/min oxygen and 120 cm^3/min helium from 50 to 500°C at either 5 or 11°C/min. A heating rate of 5°C/min was used for all the temperature-programmed oxidation spectra shown later in this report. The amount of surface carbon oxidized was calculated as described in the previous paragraph. After pulsing, the reaction was started without further treatment of the catalyst. However, after oxidation, the catalyst was reduced at 300°C for 10 min before starting the reaction again.

Infrared spectra of adsorbed carbon mon-

oxide were recorded before and after reaction. A 0.1-g sample was pressed into a 13-mm-diameter wafer and placed in a glass cell. Fresh samples were reduced in 200 cm^3/min hydrogen at 300°C for 1 h, evacuated to 1×10^{-6} Torr, and cooled to 25°C. Samples that had been exposed to heptane oxidation were immediately transferred to the infrared cell, evacuated to 1×10^{-6} Torr at 60°C for 14 h, reduced in 200 cm^3/min hydrogen at 60°C for 10 min, cooled to 25°C, and evacuated to 1×10^{-6} Torr over 30 min. Small aliquots of carbon monoxide, from 0.5 to 2.5×10^{-7} mol, were dosed into the chamber at 25°C, while recording the infrared spectrum of the sample. The intensity of the infrared bands for adsorbed carbon monoxide on the noble metal increased with dosing until the saturation point was reached (*33*). The infrared spectra shown below are for saturation only. The infrared spectra were recorded on a Digilab FTS-40 spectrometer with an MCT detector at 8 cm^{-1} resolution and coadding from 256 to 1024 scans.

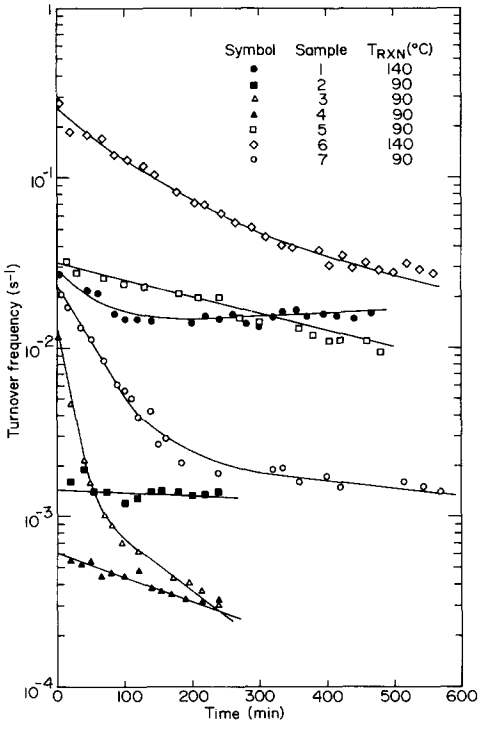

FIG. 1. The effect of time on the turnover frequencies for heptane oxidation on the platinum catalysts.

RESULTS

Rates of Reaction and Deactivation over Platinum

In Fig. 1, the specific rate of heptane oxidation over each platinum catalyst is plotted against reaction time. The turnover frequencies decrease exponentially with time. Over samples 2, 4, and 5, the slope of the line of log (turnover frequency) versus time remains constant over the whole run. However, over samples 1, 3, 6, and 7, the slope of the line drops after a certain period of time. The decay of the rate with time can be attributed to poisoning of the active sites. These sites are lost at a rate proportional to the number present, i.e., first-order deactivation (*34*)

$$\frac{d\theta}{dt} = -k\theta, \qquad (1)$$

where θ is the fraction of active sites not poisoned, t is time (s), and k is the apparent rate constant for deactivation (s^{-1}). The change in the slope of the line of log (turnover frequency) versus time, observed for some samples, suggests that there are two sites of high and low intrinsic activity

$$TOF_{Obs} = TOF_A\theta_A + TOF_B\theta_B, \qquad (2)$$

where TOF is the turnover frequency (s^{-1}), and the subscripts Obs, A and B refer to observed, A site and B site, respectively. Substitution of the integral of Eq. (1) into Eq. (2) yields

$$TOF_{Obs} = TOF_A\exp(-k_At) + TOF_B\exp(-k_Bt). \qquad (3)$$

The curves drawn through the data points in Fig. 1 are the best fit of Eq. (3) to the results. The values of the turnover frequencies and rate constants for deactivation of the A and B sites obtained from the fit are listed in Table 2.

The results presented in Fig. 1 and Table 2 reveal that the rates of heptane oxidation

TABLE 2

Rates of Heptane Oxidation and Deactivation over the Platinum Catalysts

Sample number	Composition	Initial dispersion (%)	Turnover frequency ($\times 10^{-2}$ s^{-1}) at 90°C		Deactivation rate constant ($\times 10^{-4}$ s^{-1}) at 90°C	
			TOF_A	TOF_B	k_A	k_B
1	0.4% Pt/ZrO_2	81	0.07[a]	0.05[a]	0.41[b]	−0.02[b]
2	0.3% Pt/ZrO_2	56	0.14		0.07	
3	5.0% Pt/ZrO_2	19	1.10	0.14	11.00	1.10
4	0.3% Pt/Al_2O_3	58	0.06		0.53	
5	0.8% Pt/Al_2O_3	13	3.20		0.38	
6	0.8% Pt/Al_2O_3	6	0.90[a]	0.19[a]	0.22[b]	0.03[b]
7	5.0% Pt/Al_2O_3	10	2.00	0.24	2.00	0.16

[a] Extrapolated from 140 to 90°C using an activation energy of 19 kcal/mole.

[b] Extrapolated from 140 to 90°C using an activation energy of 11 kcal/mole.

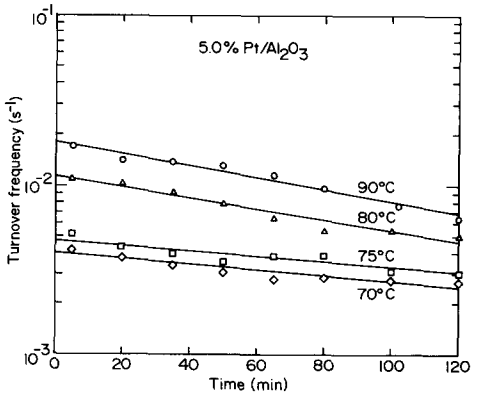

FIG. 2. The effect of time and temperature on the turnover frequency for heptane oxidation on 5.0% Pt/Al_2O_3, sample 7.

vary over a wide range. The turnover frequencies for heptane oxidation at 90°C on the *A* sites increase by a factor of 53 from the least active to the most active catalyst. The activity of the *A* sites correlates with the platinum dispersion. Samples 1, 2, and 4, with dispersions between 56 and 81%, exhibit turnover frequencies between 0.06 and 0.14 $\times$ 10^{-2} s^{-1}. Whereas samples 3, 5, 6, and 7, with dispersions between 6 and 19%, exhibit turnover frequencies between 0.9 and 3.2 $\times$ 10^{-2} s^{-1}. The turnover frequencies of the *B* sites fall within a narrow range, from 0.05 to 0.24 $\times$ 10^{-2} s^{-1}. The activity of these sites is similar to the activity of the *A* sites on the highly dispersed platinum.

As shown in the table, a large variation in the rate constants for deactivation of the *A* and *B* sites is also observed. The rate constants for deactivation of the *A* sites correlate with the metal loading. Samples 3 and 7, containing 5.0% platinum, exhibit rate constants between 2.0 and 11.0 $\times$ 10^{-4} s^{-1}. By contrast, samples 1, 2, 4, 5, and 6, containing between 0.3 and 0.8% platinum, exhibit rate constants between 0.07 and 0.53 $\times$ 10^{-4} s^{-1}.

The effect of temperature on the rates of reaction and deactivation of 5.0% Pt/Al_2O_3, sample 7, and 0.3% Pt/ZrO_2, sample 2, is shown in Figs. 2 and 3, respectively. The *y*-intercepts are the turnover frequencies of the *A* sites at each temperature. An Arrhenius plot of the turnover frequencies against temperature is presented in Fig. 4. The apparent activation energies for heptane oxidation are 20 ± 4 kcal/mole for 5.0% Pt/Al_2O_3 and 19 ± 2.5 kcal/mole for 0.3% Pt/ZrO_2 (1 kcal = 4.186 kJ). These activation energies are the same within experimental error. This suggests that the kinetics and mechanism of heptane oxidation may be the

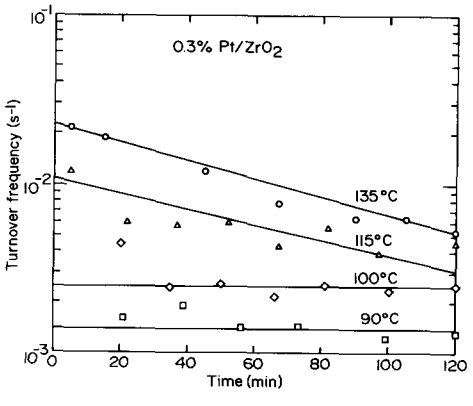

FIG. 3. The effect of time and temperature on the turnover frequency for heptane oxidation on 0.3% Pt/ZrO_2, sample 2.

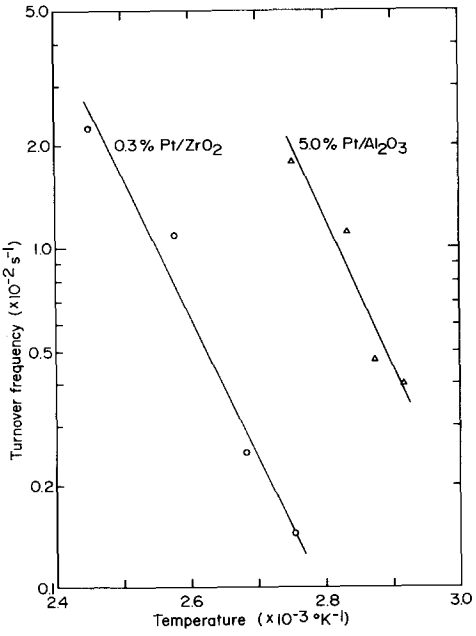

FIG. 4. The effect of temperature on the turnover frequencies of the *A* sites on 5.0% Pt/Al_2O_3, sample 7, and 0.3% Pt/ZrO_2, sample 2.

same on these two samples. The difference in turnover frequencies may be due to a difference in the density of active sites.

The slopes of the lines in Figs. 2 and 3 yield the rate constants for deactivation of the *A* sites of 5.0% Pt/Al_2O_3 and 0.3% Pt/ZrO_2. At the same temperature, the former catalyst exhibits a rate of deactivation much higher than that of the latter catalyst. In fact at 90 and 100°C, 0.3% Pt/ZrO_2 shows no appreciable loss of activity with time. An Arrhenius plot of the deactivation rate constants for 5.0% Pt/Al_2O_3 yields an activation energy of 11 ± 4 kcal/mole.

The effect of the partial pressures of heptane and oxygen on the rates of reaction and deactivation of 5.0% Pt/Al_2O_3 are summarized in Table 3. The oxygen pressure was varied while maintaining a stoichiometric excess of oxygen. However, the heptane pressure was varied widely from lean to rich conditions. Within the uncertainty of the limited measurements made, the rates of oxidation and deactivation are zero order in heptane pressure and zero order in oxygen pressure.

TABLE 3

Partial Pressure Dependence of the Rates of Heptane Oxidation and Deactivation over 5.0% Pt/Al_2O_3 at 90°C

Partial pressures (Torr)		Turnover frequency of *A* sites ($\times 10^{-2}$ s^{-1})	Deactivation rate constant ($\times 10^{-4}$ s^{-1})
Heptane	Oxygen		
5	80	1.7	1.0
5	245	2.0	1.6
5	440	0.9	0.8
20	245	2.0	2.0
65	245	2.4	1.8
Order in oxygen		−0.3 ± 0.4	−0.1 ± 0.4
Order in heptane		+0.1 ± 0.1	+0.1 ± 0.1

Rates of Reaction and Deactivation over Palladium

The specific rate of heptane oxidation over each palladium catalyst is plotted against reaction time in Fig. 5. The palladium catalysts show the same exponential

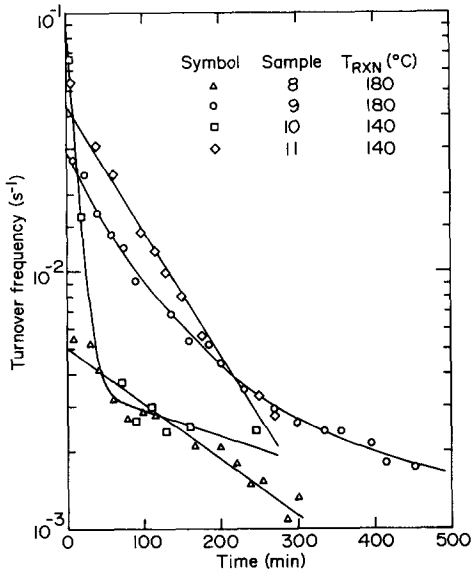

FIG. 5. The effect of time on the turnover frequencies for heptane oxidation on the palladium catalysts.

TABLE 4

Rates of Heptane Oxidation and Deactivation over the Palladium Catalysts

Sample number	Composition	Initial dispersion (%)	Reaction temperature (°C)	Turnover frequency ($\times 10^{-2}$ s^{-1}) at T_{rxn}		Deactivation rate constant ($\times 10^{-4}$ s^{-1}) at T_{rxn}	
				TOF_A	TOF_B	k_A	k_B
8	0.2% Pd/Al_2O_3	81	180	0.5		0.8	
9	0.2% Pd/Al_2O_3	55	180	2.4	0.62	2.9	0.46
10	2.3% Pd/Al_2O_3	10	140	9.4	0.36	17.5	0.37
11	2.3% Pd/Al_2O_3	3	140	4.3		1.8	

decay of the rate as observed for the platinum catalysts. The curves drawn in the figure are the best fit of Eq. (3) to the data points. The turnover frequencies and deactivation rate constants of the *A* and *B* sites are presented in Table 4. These results indicate that the rate of heptane oxidation depends on the palladium dispersion. The 0.2% Pd/Al_2O_3 samples, with dispersions of 55 and 81%, exhibit turnover frequencies of the *A* sites between 0.5 and 2.4 $\times$ 10^{-2} s^{-1} at 180°C. By contrast, the 2.3% Pd/Al_2O_3 samples, with dispersions of 3 and 10%, exhibit turnover frequencies of the *A* sites between 4.3 and 9.4 $\times$ 10^{-2} s^{-1} at 140°C. If these latter samples were tested at 180°C, the turnover frequencies would be much higher. The rate constants for deactivation of the *A* sites follow a trend parallel to that of the turnover frequencies. The rate constants for deactivation of the 0.2% Pd/Al_2O_3 samples at 180°C are on average lower than those of the 2.3% Pd/Al_2O_3 samples at 140°C.

The activities of all the catalysts can be compared by extrapolating the rate measurements to the same temperature using an apparent activation energy of 19 kcal/mole. This calculation yields the following average turnover frequencies of the *A* sites at 140°C: 0.02 s^{-1} for platinum particles with dispersions about 50% (samples 1, 2, and 4), 0.45 s^{-1} for platinum particles with dispersions below 20% (samples 3, 5, 6, and 7), 0.002 s^{-1} for palladium particles with dispersions above 50% (samples 8 and 9), and 0.07 s^{-1} for palladium particles with dispersion below 10% (samples 10 and 11). The rate of heptane oxidation is about 8 times higher on platinum compared to palladium, and about 29 times higher on poorly dispersed particles compared to highly dispersed ones.

Change in Metal Sites during Reaction

The number of accessible metal sites on the catalysts after exposure to reaction conditions was determined by adsorption of hydrogen, oxygen, and carbon monoxide. Periodically throughout a run, the feed was switched from the reaction mixture to helium and the reactor cooled to 60°C. After a 1-h purge in helium, the sample was exposed to repeated pulses of the different gases, and the amount adsorbed recorded with the gas chromatograph. Unfortunately, the heptane concentration decreased slowly after switching to the helium. The heptane in the purge gas may have titrated away any adsorbed oxygen, then decomposed on the exposed metal to adsorbed carbon.

After exposure to heptane oxidation (and the helium purge), the catalysts adsorb carbon monoxide and hydrogen, but not oxygen. During carbon monoxide pulsing, less than 10% of the gas adsorbed is liberated as carbon dioxide. Conversely, when the adsorbed carbon monoxide is titrated with oxygen, nearly quantitative conversion to carbon dioxide is observed. These results

TABLE 5

Changes in the Metal Dispersions of the Catalysts with Exposure to Heptane Oxidation

Sample number	Composition	Dispersion (%)			
		Before reaction	After reaction		After regeneration[a]
			H_2–O_2	CO	
2	0.3% Pt/ZrO_2	56	50	56	56
3	5.0% Pt/ZrO_2	19	4	11	14
4	0.3% Pt/Al_2O_3	58	23	51	60
5	0.8% Pt/Al_2O_3	13	6	10	12
7	5.0% Pt/Al_2O_3	10	6	8	10
11	2.3% Pd/Al_2O_3	3	3	3	3

[a] The samples were regenerated after reaction by oxidation at 500°C for 20 min and reduction at 300°C for 20 min.

indicate that only a small portion of the metal surface is initially covered with oxygen. Most of the metal surface is initially covered with carbon. Part of this carbon can be displaced by carbon monoxide and hydrogen, whereas none of it is displaced by oxygen. Results very similar to these are obtained if a fresh catalyst is exposed to 20 Torr of heptane at 90°C for 2 h, and then titrated with the different gases.

Shown in Table 5 is the change in metal dispersions of the catalysts with exposure to reaction conditions. The dispersions were determined by hydrogen and oxygen titration and by carbon monoxide displacement of adsorbed hydrogen:

$$\tfrac{3}{2}H_2 + {}^*O \rightarrow H_2O + {}^*H. \quad (4)$$

$$\tfrac{3}{4}O_2 + {}^*H \rightarrow \tfrac{1}{2}H_2O + {}^*O. \quad (5)$$

$$CO + {}^*H \rightarrow \tfrac{1}{2}H_2 + {}^*CO. \quad (6)$$

The * means a metal site. Before reaction and after regeneration, the dispersions calculated from Eqs. (4)–(6) are the same within experimental error, so only one entry is provided in the table. However, after reaction, significantly different values are calculated from Eqs. (4) and (5) compared to Eq. (6). Dispersions measured by hydrogen and oxygen titration can be more than 50% below those measured by carbon monoxide adsorption. These results indicate that the carbon monoxide displaces a greater fraction of the adsorbed carbon than does the hydrogen and oxygen.

Comparison of the dispersion measured after reaction by carbon monoxide adsorption to the dispersion measured after regeneration reveals that most of the carbon deposited during heptane oxidation can be displaced from the metal surface. The percentage of the metal sites accessible to carbon monoxide varies from 80 to 100%. The dispersions presented in Table 5 are the average of several measurements taken throughout the run. Catalysts were titrated at different times ranging from 5 min to 8 h after the start of the reaction. In all cases, no change in the gas uptakes is observed with reaction time.

Oxygen titration of the catalysts after reaction is sensitive to the previous exposure to hydrogen. The oxygen uptake is much greater if hydrogen is flowed continuously

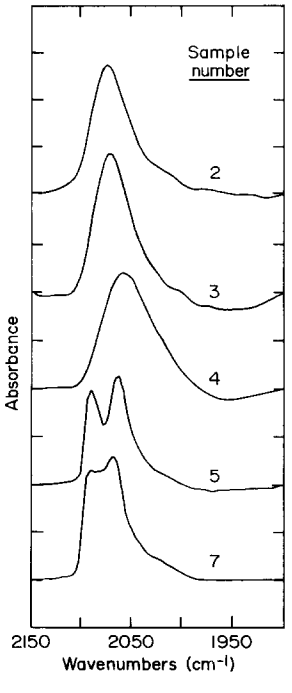

FIG. 6. Infrared spectra of adsorbed carbon monoxide on the platinum catalysts before heptane oxidation.

TABLE 6

Characteristics of the Infrared Spectra of Adsorbed Carbon Monoxide on the Platinum Catalysts

Sample number	Composition	Initial dispersion (%)	Frequency of infrared band (cm^{-1})		Full-width at half-maximum (cm^{-1})	
			Before reaction	After reaction	Before reaction	After reaction
2	0.3% Pt/ZrO_2	56	2076	2076	40	40
3	5.0% Pt/ZrO_2	19	2075	2079	40	40
4	0.3% Pt/Al_2O_3	58	2060	2052,2074sh	55	68
5	0.8% Pt/Al_2O_3	13	2066,2091	2066	44	50
7	5.0% Pt/Al_2O_3	10	2069,2091sh	2065	44	50

over the sample instead of pulsed over the sample. For example, the uptake of oxygen on 5.0% Pt/Al_2O_3, sample 7, is 8 times greater after flowing hydrogen for 10 min at 60°C compared to pulsing hydrogen to saturation. Oxygen pulsing after a hydrogen flow produces a large quantity of carbon dioxide. Most of the increased oxygen uptake can be accounted for in the carbon dioxide. A plausible explanation for these results is as follows: When hydrogen is flowed over the catalyst, surface carbon is hydrogenated by hydrogen spillover from the metal particles. This hydrogenated carbon is more reactive and is titrated away by oxygen at 60°C.

Infrared spectra of adsorbed carbon monoxide were recorded before and after reaction to see if more could be learned about the carbon covering the metal surface. The spectra obtained before reaction for samples 2, 3, 4, 5, and 7 are shown in Fig. 6. The frequencies and full-width at half-maxima (FWHM) are listed in Table 6. The 0.3% Pt/ZrO_2 and 5.0% Pt/ZrO_2 catalysts, samples 2 and 3, exhibit identical infrared spectra for adsorbed carbon monoxide. One symmetric peak is observed at 2076 cm^{-1} with an FWHM of 40 cm^{-1}. The infrared peak is the same for the two samples in spite of a large difference in platinum dispersion. The 0.3% Pt/Al_2O_3 catalyst, sample 4, exhibits a single symmetric peak at 2060 cm^{-1} with an FWHM of 55 cm^{-1}. This spectrum may be contrasted with those of 0.8% Pt/Al_2O_3 and 5.0% Pt/Al_2O_3, samples 5 and 7. The spectra of these last two catalysts contain two peaks at 2067 and 2091 cm^{-1}. The FWHM of the combined peak is 44 cm^{-1}, indicating that the individual peaks in these spectra are narrower than the single peak observed in the other spectra. Sample 4 differs from samples 5 and 7 in two ways: it has a much higher dispersion, and it was prepared using $Pt(NH_3)_4Cl_2$ instead of H_2PtCl_6. Excepting the difference in band position, the infrared spectrum of sample 4 is very similar to the infrared spectra of samples 2 and 3. These samples have different dispersions, but all were prepared from the platinum amine complex. The infrared peaks observed, at 2065, 2075, and 2091 cm^{-1}, are indicative of different sites for carbon monoxide adsorption on the platinum. These data indicate that the relative concentrations of these sites depends on the metal salt used and the support composition.

The infrared spectra of adsorbed carbon monoxide recorded after reaction are shown in Fig. 7. The band frequencies and widths are listed in Table 6. No changes in the infrared spectra are observed following exposure of samples 2 and 3 to reaction conditions. However, samples 4, 5, and 7 show pronounced changes in the distribution of bands after reaction. A shoulder at 2073 cm^{-1} has appeared in the infrared spectrum of sample 4. In the infrared spectra of samples 5 and

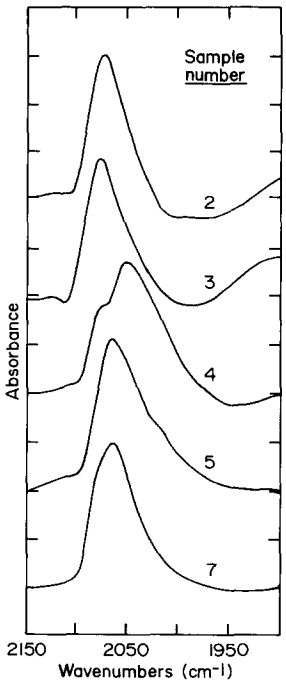

FIG. 7. Infrared spectra of adsorbed carbon monoxide on the platinum catalysts after heptane oxidation.

6, the peak at 2091 cm^{-1} has disappeared, whereas the peak at 2065 cm^{-1} has become larger and broader. Apparently, the sites giving rise to the 2091 cm^{-1} peak are sensitive to the presence of carbon on the surface, whereas the peaks at 2076 and 2060 cm^{-1} are not.

Accumulation of Carbon during Reaction

Temperature-programmed oxidation spectra were obtained after exposing the catalysts to heptane oxidation for different periods of time. These experiments reveal that a large quantity of carbon deposits on the catalysts during heptane oxidation. The spectra recorded of 5.0% Pt/Al_2O_3 are shown in Fig. 8. The area under the curve times the heating rate equals the total amount of carbon oxidized off the sample. The carbon removed after 240 min of reaction at 90°C is 1.2×10^{-3} mole/g. This is 10 times greater than the carbon removed from the freshly oxidized and reduced sample, and is 45 times greater than the moles of platinum exposed. The amount of carbon deposited during heptane oxidation exceeds that deposited when the catalyst is exposed to heptane alone. After 240 min in 20 Torr of heptane at 90°C, 2.7×10^{-4} mole/g of carbon are removed by oxidation. Carbon also deposits directly on the alumina support, but at a much slower rate. After 120 min of reaction at 90°C, the quantities of carbon oxidized off Al_2O_3 and 5.0% Pt/Al_2O_3 are 0.7 and 7.0×10^{-4} mole/g, respectively.

Shown in Fig. 9 are temperature-programmed oxidation spectra for about half the catalysts and both supports. Table 7 lists the temperatures of maximum oxidation rate. The spectra for the platinum on zirconia catalysts, samples 2 and 3, and the zirconia support are similar. A single symmetric peak is observed between 300 and 400°C. This peak shifts down from 370 to 320 to 295°C as the metal loading increases from 0 to 0.3 to 5.0%. These spectra are in strong contrast to those obtained for the platinum on alumina catalysts, samples 4, 5, and 7, and the alumina support. At metal loadings between 0 and 0.8% on alumina, the TPO spectrum consists of a broadband extending from 100 to 500°C. The peak maximum shifts down from 450 to 400 to 345°C as the weight of platinum increases from 0 to 0.3 to 0.8%. For 5.0% Pt/Al_2O_3, a sharp peak at 200°C

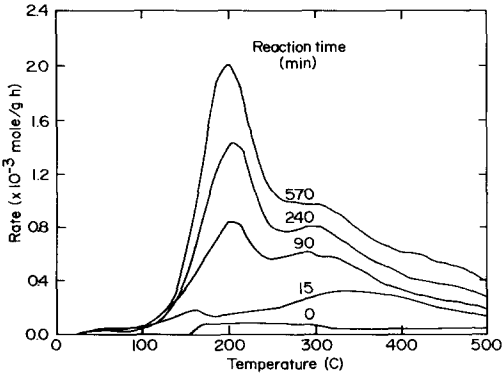

FIG. 8. Temperature-programmed oxidation of 5.0% Pt/Al_2O_3, sample 7, following different times of exposure to heptane oxidation.

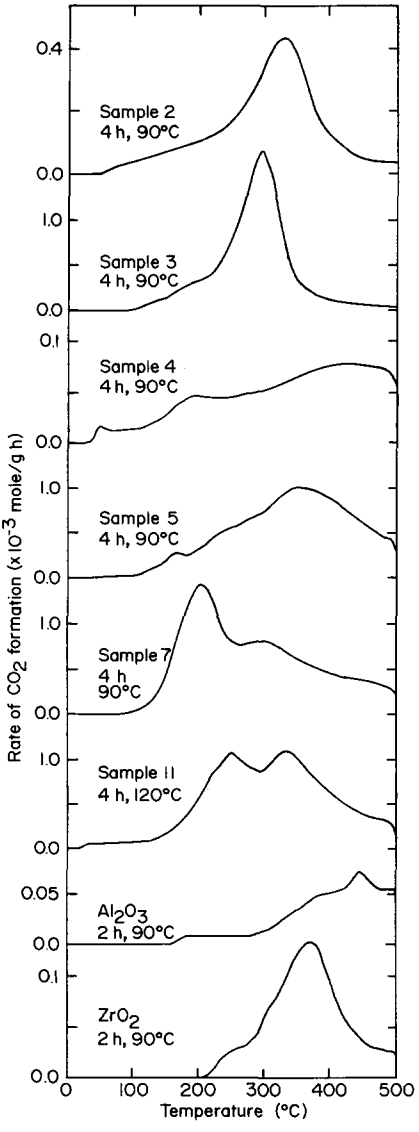

FIG. 9. Temperature-programmed oxidation of the platinum and palladium catalysts and the supports. The time and temperature of heptane oxidation are given below the sample number.

has grown in on top of the broadband. The difference between the spectra of 0.8% and 5.0% Pt/Al_2O_3 must be due to the metal loading, since these catalysts were prepared the same way and have similar dispersions. The 2.3% Pd/Al_2O_3 catalyst, sample 11, exhibits a broadband like the Pt/Al_2O_3 catalysts. However, in this case, two temperature maxima are observed at 250 and 335°C. In summary, the rate of oxidation of the surface carbon strongly depends on the composition of the support, the composition of the metal and the amount of metal deposited.

Shown in Table 7 is the amount of adsorbed carbon converted to carbon dioxide by temperature-programmed oxidation. The quantity of carbon deposited during heptane oxidation correlates with the metal dispersion. After reaction, only a small amount of carbon is removed from the catalysts with dispersions greater than 50%, samples 2 and 4. The amount of carbon oxidized off these samples is not much different than the amount oxidized off the supports. By contrast, a much larger amount of carbon is removed from the catalysts with dispersions below 20%, samples 3, 5, 7, and 11. The catalysts which are active for coke formation are also active for heptane oxidation. As shown in Tables 2 and 4, the turnover frequencies of samples 2 and 4 at 90°C are near 0.001 s^{-1}, whereas the turnover frequencies of samples 3, 5, and 7 at 90°C and 11 at 120°C are near 0.02 s^{-1}.

On samples 2, 7, and 11, a series of temperature-programmed oxidation spectra were collected after different periods of heptane oxidation. The amount of carbon oxi-

TABLE 7

Temperature-Programmed Oxidation of the Platinum and Palladium Catalysts[a]

Sample number	Composition	Initial dispersion (%)	Temperature (°C) of maximum rate	Carbon oxidized ($\times 10^{-4}$ mole/g)	
				Before reaction	After reaction
2	0.3% Pt/ZrO_2	56	320	0.3	2.4
3	5.0% Pt/ZrO_2	19	295	1.1	6.4
4	0.3% Pt/Al_2O_3	58	400	0.2	1.0
5	0.8% Pt/Al_2O_3	13	345	0.0	8.9
7	5.0% Pt/Al_2O_3	10	200,300sh	1.1	11.6
11	2.3% Pd/Al_2O_3	3	250,335	0.1	9.1
	Al_2O_3		450	0.3	0.7
	ZrO_2		370	0.3	0.8

[a] The spectra were obtained after exposure to heptane oxidation at the following conditions: 4 h at 90°C for the Pt samples; 4 h at 120°C for the Pd samples; and 2 h at 90°C for the supports.

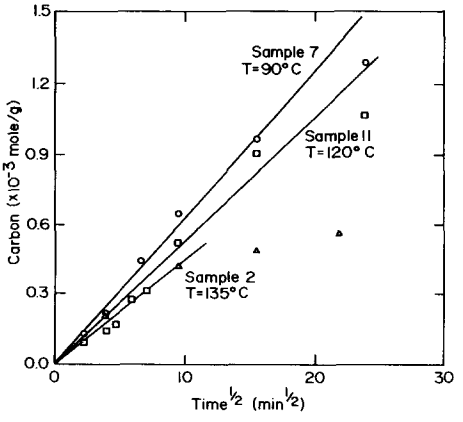

FIG. 10. The dependence of the amount of carbon deposited on the square root of reaction time for samples 2, 7, and 11. The reaction temperature is given below the sample number.

dized is plotted against the square root of reaction time in Fig. 10. Most of the data fall along a straight line. For sample 2, the rate of carbon accumulation falls below the half-order dependence starting at 120 min of reaction. This may be related to a change in the catalyst activity, since the rate constant for deactivation dropped at the same time. The square-root dependence of the quantity of adsorbed carbon on reaction time suggests that its rate of accumulation is controlled by surface diffusion. A likely scenario is that heptane decomposes to adsorbed carbon and hydrogen on the metal crystallites. Some of the adsorbed carbon is oxidized to carbon dioxide, while the remainder migrates to the support. The majority of the carbon removed by temperature-programmed oxidation comes from the support.

DISCUSSION

Composition and Structure of the Metal Particles

The large variation in turnover frequencies indicates that the rate of heptane oxidation depends on the composition and structure of the metal particles. These properties of the catalysts are considered next.

During hydrocarbon oxidation, it is possible for the platinum and palladium particles to be oxidized to PtO_2 and PdO (*10, 13, 14, 19*). This can affect the catalytic activity. In the present study, the reaction temperatures are too low to oxidize either metal. The highest reaction temperatures used are 140°C for platinum and 180°C for palladium. Small platinum and palladium crystallites begin oxidizing in air at 300 and 200°C, respectively (*13, 14, 35, 36*). Also, the uptakes of hydrogen, oxygen, and carbon monoxide after reaction are almost the same as those on the freshly reduced samples. If the metal were oxidized, much larger uptakes of hydrogen and carbon monoxide would be observed with significant production of carbon dioxide in the latter case.

Three different surface structures are evident on the reduced platinum particles. These structures give rise to three bands at 2065, 2075, and 2091 cm^{-1} in the infrared spectrum of adsorbed carbon monoxide. These bands have been observed before on supported platinum catalysts (*13, 37–39*). They also have been observed on stepped Pt(111) single crystals (*40*). The 2065 cm^{-1} peak is detected at the lowest coverage of carbon monoxide on the single crystal. As the coverage increases, the step sites fill up and the peak shifts to 2075 cm^{-1}. With further increases in coverage, the terrace sites fill, and the 2075 cm^{-1} peak disappears, while a second peak appears at 2085 cm^{-1}. The 2085 cm^{-1} peak shifts to 2095 cm^{-1} upon increasing the coverage to one monolayer. The band assignments for the single crystal surface may be summarized as follows: 2065 cm^{-1}, isolated carbon monoxide molecule on the surface; 2075 cm^{-1}, high coverage of carbon monoxide on low coordination sites; and 2095 cm^{-1}, high coverage of carbon monoxide on surfaces containing Pt(111) terraces. On supported platinum catalysts, the three peaks are attributable to different crystallite structures, since all three are observed at saturation coverage of carbon monoxide. The proposed band assignments for the supported platinum catalysts are: 2065 cm^{-1}, carbon monoxide on

isolated metal atoms or on very small metal particles; 2075 cm^{-1}, carbon monoxide on small metal particles, or on large metal particles exposing mainly low coordination sites; and 2991 cm^{-1}, carbon monoxide on large particles with (111) facets.

Comparison of Table 1 with Table 6 reveals that the infrared spectra correlate with the support composition and method of catalyst preparation. The platinum on zirconia catalysts, samples 2 and 3, are prepared by impregnation with the amine salt, oxidation at 500°C, and reduction at 300°C. These catalysts exhibit an infrared band at 2075 cm^{-1} consistent with either small particles or large particles with rough surfaces. High-resolution electron micrographs are being obtained of the large particles to try and confirm this morphology. The highly dispersed platinum on alumina, sample 4, is prepared by impregnation with the amine salt, oxidation at 500°C, and reduction at 300°C. This catalyst exhibits an infrared peak at 2060 cm^{-1} indicative of very small metal particles. The platinum on alumina catalysts of low dispersion, samples 5 and 7, are prepared by impregnation with the chloride salt, oxidation at 600°C, and reduction at 300°C. These catalysts exhibit peaks at 2065 and 2091 cm^{-1} characteristic of a bimodal distribution of small metal particles and large metal particles with (111) facets. This distribution of sizes is confirmed by electron microscopy. An electron micrograph of 5.0% Pt/Al_2O_3, sample 7, is shown in Fig. 11. Clearly evident are two sizes of platinum crystallites above 50 Å and below 20 Å in diameter.

The two sizes of platinum particles on alumina have been observed previously (*13, 39, 41*). In these studies, the small and large crystallites have been referred to as the dispersed and crystallite phases of platinum, respectively. The dispersed phase is formed by the adsorption of $PtCl_6^{-2}$ onto alumina, followed by low-temperature oxidation and reduction. When the samples are oxidized at temperatures above 500°C, large crystallites are formed from the small ones. This produces the bimodal distribution of particle sizes, which in turn give rise to the low and high frequency bands in the infrared spectrum of adsorbed carbon monoxide (*39*).

After exposure to heptane oxidation, the Pt/Al_2O_3 catalysts of low dispersion no longer exhibit the infrared band at 2091 cm^{-1}, whereas the infrared band at 2065 cm^{-1} has grown in intensity. This cannot be due to the break up of large particles into small ones, because the gas uptakes indicate the particles are still of low dispersion. A more likely explanation is that the adsorbed carbon breaks up the ordering of the adsorbed carbon monoxide molecules on the (111) facets, so that their vibrational frequency shifts down from 2091 to 2065 cm^{-1}.

To summarize, a wide range of crystallite sizes and structures are exhibited by the platinum catalysts. Samples 1, 2, and 4 contain highly dispersed, small metal particles, $d < 20$ Å. Sample 3 contains large metal particles, $d > 50$ Å, which may have rough surfaces. Samples 5, 6, and 7 contain both small metal particles, $d < 20$ Å, and large metal particles, $d > 50$ Å, with (111) facets. Most of the surface platinum in these latter three catalysts is associated with the large particles.

The structures of the palladium catalysts have not been characterized as carefully. Nevertheless, the palladium dispersions suggest that samples 8 and 9 contain small metal particles, $d < 20$ Å, while samples 10 and 11 contain large metal particles, $d > 50$ Å. Electron micrographs have been taken of sample 10 and they indicate that the palladium crystallite sizes vary from 50 to 135 Å in diameter.

Structure Sensitivity of Heptane Oxidation

The turnover frequency for heptane oxidation on the *A* sites depends on the composition of the metal and on the metal particle size. At 140°C, platinum crystallites are 8 times more active than palladium crystallites in the same size range. Platinum crystallites larger than 50 Å in diameter are 20

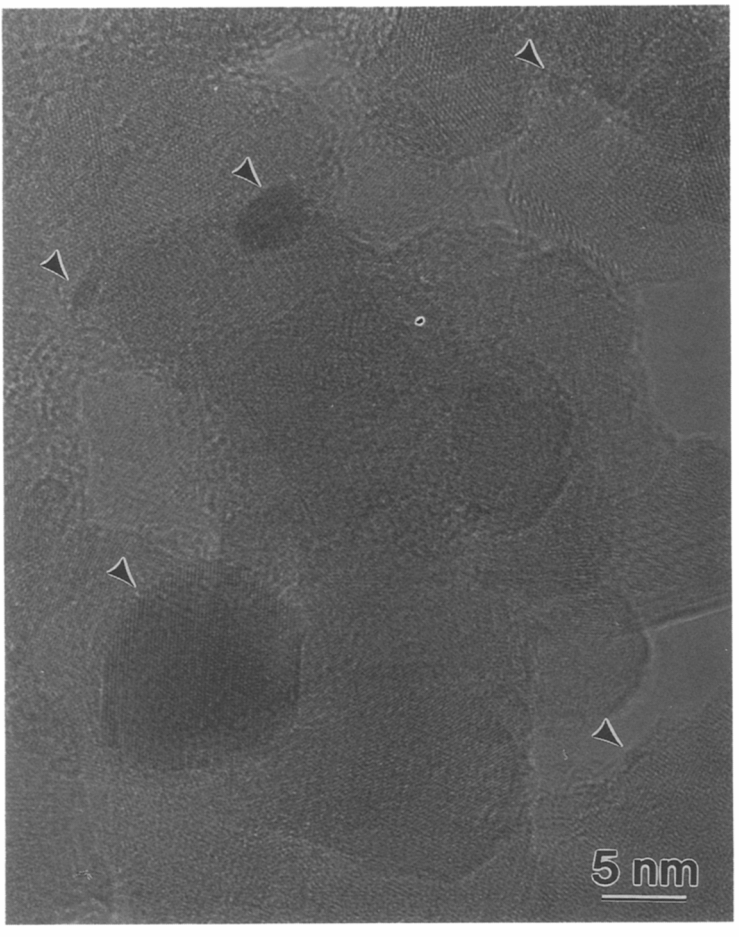

FIG. 11. A transmission electron micrograph of 5.0% Pt/Al_2O_3, sample 7, at 500,000 magnification. The arrows point to small and large platinum particles.

times more active than platinum crystallites smaller than 20 Å in diameter. A similar effect of particle size is observed for palladium. The change in the turnover frequency of the *A* sites with particle size appears to be due to a change in the density of active sites, and not the mechanism or energetics of the reaction. This idea is consistent with measuring the same apparent activation energy for heptane oxidation on catalysts of low and high metal dispersion (see Fig. 4).

The turnover frequency for heptane oxidation on the *B* sites depends on the composition of the metal and somewhat on the metal particle size. At 140°C, platinum crystallites are about 10 times more active than palladium crystallites of similar size. On platinum, the large particles are only 4 times more active than small ones. The *B* sites are the sites on the large particles which remain after deactivation. As can be seen in Table 2, the *B* sites on the large particles oxidize heptane at about the same rate as the *A* sites on the small particles. It is possible that both of these sites are associated with the same surface structures, such as facet edges and corners and defects.

The results obtained here can be compared to other studies of hydrocarbon oxidation over reduced metal catalysts. Similar

rate differences between platinum and palladium have been reported by others. Yu Yao (*10*) found that at 140°C in excess oxygen, platinum wire oxidized butane 6 times faster than palladium wire. Drozdov *et al.* (*15*) found that at 345°C in excess oxygen, platinum black oxidized butane 8 times faster than palladium black. The effect of particle size was examined in both of these studies. However, it is unclear whether the supported metal particles are oxidized or reduced under their reaction conditions. Carballo and Wolf (*27*) examined the effect of crystallite size on propylene oxidation over reduced Pt/Al_2O_3 catalysts. At 130°C in excess oxygen, 144 Å particles are 6 times more active than 11 Å particles. This variation is in the same direction, but smaller than that observed for heptane oxidation.

Carbon Fouling of the Metal Particles

The deactivation of the catalysts is due to carbon fouling of the metal particles. The deactivation rate is first order in active sites (Eq. (1)). These kinetics are consistent with the sites becoming covered by coke from the oxidative dehydrogenation of heptane. After reaction, temperature-programmed oxidation confirms that carbon builds up on the catalysts throughout the run. Oxidizing off the carbon restores the catalysts to their initial activity.

The kinetics of coke formation differ from the kinetics of deactivation. As shown in Fig. 10, the carbon buildup follows a half-order dependence on time. By contrast, the active sites foul at an exponential rate. A half-order dependence on time is often observed for coke formation during catalytic reactions (*42*). Voorhies (*43*) first reported this relationship for coking during catalytic cracking. In the present case at least, the half-order dependence on time is due to a diffusion-controlled process. Carbon formed on the metal particles migrates slowly to the support.

The carbon that migrates to the support is obviously not the carbon that fouls the metal particles. This is why the kinetics of coke formation and deactivation are different. The carbon which fouls the metal particles seems to be only a single adsorbed layer. Otherwise it would not be possible to displace this carbon from the surface by adsorption of hydrogen and carbon monoxide at 60°C. The number of active sites on the metal surface may critically depend on the relative concentrations of adsorbed carbon and oxygen. Deactivation may occur by carbon slowly displacing oxygen from the surface during reaction. Unfortunately, inherent limitations in the pulse-adsorption technique prevented us from measuring the distribution of carbon and oxygen on the metal surfaces following reaction.

During temperature-programmed oxidation, carbon migrates from the support back to the metal particles, where it is converted to carbon dioxide. This is evidenced by the strong dependence of the oxidation rate on metal loading and support composition. As shown in Table 7, the temperature of maximum oxidation rate on Pt/ZrO_2 shifts from 370 to 320 to 295°C upon increasing the platinum loading from 0 to 0.3 to 5.0%. An analogous downward shift in temperature occurs with increasing metal loading on Pt/Al_2O_3. The oxidation rate accelerates as the density of metal crystallites on the support rises, because the distance the carbon atoms diffuse before reacting shrinks. Comparison of 5% Pt/Al_2O_3 with 5% Pt/ZrO_2 reveals that the former catalyst exhibits a much lower temperature of maximum oxidation rate. The platinum on zirconia has a higher density of metal crystallites due to the higher metal dispersion and lower support surface area. Evidently, the carbon migration rate across the alumina is much faster than that across the zirconia, or the carbon on the alumina occupies sites closer to the platinum particles.

The amounts of coke laid down during reaction and the rates of deactivation of the catalysts show a similar dependence on metal particle size. The highly dispersed metal catalysts exhibit lower amounts of carbon deposited (Table 7) and lower deacti-

TABLE 8

Comparison of the Carbon Accumulation Rate with the Deactivation Rate over the Platinum Catalysts of Low Dispersion

Sample number	Composition	Initial dispersion (%)	Net carbon[a] ($\times 10^{-4}$ mole/g)	C/Pt_s[b]	Deactivation rate constant, k_A ($\times 10^{-4}$ s^{-1})
3	5.0% Pt/ZrO_2	19	4.8	10	11.00
5	0.8% Pt/Al_2O_3	13	8.5	130	0.38
7	5.0% Pt/Al_2O_3	10	10.1	51	2.00

[a] Net carbon, net moles carbon deposited on catalyst minus net moles carbon deposited on support.

[b] C/Pt_s, net moles carbon deposited divided by moles surface platinum.

vation rate constants of the *A* sites (Table 2) than the poorly dispersed metal catalysts. These results indicate that small metal particles are relatively inactive for coke formation, and as a result, deactivate slowly if at all. A similar effect of particle size on the coke deposition rate is observed for hydrocarbon reforming over platinum (*44*). However, in this case, significant amounts of carbon accumulate on catalysts containing both large and small metal particles, and both large and small metal particles deactivate by carbon fouling.

On the catalysts containing large metal particles, the rates of coke formation and deactivation depend on the amount of metal on the support and the support composition. In Table 8, the moles of carbon deposited per mole of platinum exposed, C/Pt_s, and the deactivation rate constant of the *A* sites, k_A, are shown for the three platinum catalysts with dispersions below 20%. The 0.8 and 5.0% Pt/Al_2O_3 catalysts exhibit nearly the same dispersion, so that the latter sample contains about 6 times more metal crystallites per unit area of support. The catalyst with the lower density of metal crystallites accumulates 2.5 times more carbon per surface platinum atom, and it deactivates at a 5.3 times slower rate. Thus, the rate of carbon accumulation normalized to the metal surface area correlates inversely with the rate of deactivation. A similar trend is observed when the effect of the support is considered. The 5.0% Pt/Al_2O_3 accumulates 5 times more carbon per surface platinum atom and deactivates at a 5.5 times slower rate than the 5.0% Pt/ZrO_2. These trends can be explained as follows. Carbon produced on the metal particles either oxidizes to carbon dioxide, migrates to the support, or fouls an active site. The faster the carbon diffuses from the metal to the support, the slower the catalyst deactivates. Decreasing the density of metal crystallites increases the diffusion rate and decreases the deactivation rate. Switching from zirconia with 40 m^2/g surface area to alumina with 83 m^2/g surface area increases the diffusion rate and decreases the deactivation rate.

The rates of heptane oxidation and deactivation follow zero-order dependencies on the heptane and the oxygen partial pressures. The amount of carbon accumulated on the catalyst is also insensitive to the pressure of heptane and oxygen. These kinetics are consistent with fast adsorption of heptane and oxygen followed by slow surface reaction. The coke formed upon heptane adsorption chooses between three parallel slow paths: oxidation to carbon dioxide, migration to the support, or fouling of an active site. A logical choice for the active sites is the interface between adsorbed carbon and oxygen on the metal surface. At the interface, carbon and oxygen are converted to carbon dioxide, thereby creating vacant sites for adsorption of another heptane molecule. The adsorption energies of heptane and oxygen may be more closely matched on large particles compared to small ones, so that the large particles contain many more sites where carbon and oxygen are adjacent. Since carbon oxidation, migration, and fouling are parallel slow paths, large particles exhibit higher turnover frequencies for heptane oxidation, higher rates of carbon accumulation, and if carbon migration to the support is slow, higher rates of deactivation.

This study has revealed an important role for the support in low-temperature hydrocarbon oxidation over precious metals. The

support provides a place for coke to accumulate without interfering with the oxidation sites on the metal. If the support surface area increases relative to the metal surface area, the performance of the catalyst is vastly improved. This is easily seen by comparing the turnover frequency versus time curves for 0.8% Pt/Al_2O_3, sample 5, and 5.0% Pt/Al_2O_3, sample 7, in Fig. 2. Sample 5 with the lower density of platinum crystallites maintains high activity over a period of time much longer than that of sample 7.

CONCLUSIONS

The platinum and palladium catalysts are fouled by carbon during heptane oxidation at low temperature. The deactivation rate is first-order in active sites. On some catalysts, two sites are present, *A* and *B* sites, with correspondingly high and low rate constants for deactivation. On 5.0% Pt/Al_2O_3, the rate constant for deactivation of the *A* sites exhibits an 11 kcal/mole activation energy, and does not depend on the heptane or oxygen partial pressures.

The rate of carbon accumulation on the catalysts follows a half-order dependence on time, indicative of a diffusion-controlled process. Most of the carbon generated on the metal migrates to the support and does not foul the metal surface. The coke formation rate and the deactivation rate depend on the catalyst composition and structure. Small platinum crystallites, $d < 20$ Å, deposit much less carbon and deactivate much more slowly than large platinum crystallites, $d > 50$ Å. On large platinum crystalites, coking and deactivation are sensitive to the number of metal particles on the support and the support composition. Increasing the number of metal particles on the alumina 6 times, increases the coke formation rate per surface metal atom 2.5 times, and decreases the deactivation rate 5 times. Switching from zirconia (40 m^2/g) to alumina (83 m^2/g) at 5.0% metal loading, increases the coke formation rate per surface metal atom 5 times, and decreases the deactivation rate 5.5 times. Evidently, the faster carbon diffuses from the metal to the support, the slower carbon fouls the metal surface.

The turnover frequencies for heptane oxidation on the *A* and *B* sites are moderately affected by the nature of the metal and the metal particle size. For the *A* sites, platinum is 8 times more active than palladium, and large platinum crystallites are 20 times more active than small ones. For the *B* sites, platinum is 10 times more active than palladium, and large platinum crystallites are 4 times more active than small ones. A similar affect of particle size is observed for palladium. On 5.0% Pt/Al_2O_3, the heptane oxidation rate on the *A* sites exhibits an activation energy of 19 kcal/mole, and does not depend on the heptane or oxygen partial pressures. The same activation energy is exhibited by 0.3% Pt/ZrO_2 which contains much smaller metal particles. This suggests that the change in turnover frequency with particle size is due to a change in the fraction of metal sites which are active for heptane oxidation.

ACKNOWLEDGMENTS

This research was supported by the National Science Foundation Engineering Research Center for Hazardous Substance Control at UCLA. The authors also thank David J. Smith and the High Resolution Electron Microscope Facility at Arizona State University for the pictures of the catalysts. The microscope facility was established with support from the National Science Foundation (Grant No. DMR-86-11609).

REFERENCES

1. Wei, J., *in* "Advances in Catalysis" (D. D. Eley, H. Pines, and P. B. Weisz, Eds.), Vol. 24, p. 57. Academic Press, New York, 1975.
2. Kim, G., *Ind. Eng. Chem. Prod. Res. Dev.* **21,** 267 (1982).
3. Spivey, J. J., *Ind. Eng. Chem. Res.* **26,** 2165 (1987).
4. Gandhi, H. S., and Shelef, M., *in* "Atmospheric Ozone Research and its Policy Implications" (T. Schneider, Ed.), p. 1037. Elsevier, Amsterdam, 1989.
5. Anderson, R. B., Stein, K. C., Feenan, J. J., and Hofer, L. J. E., *Ind. Eng. Chem.* **53,** 809 (1961).
6. Mezaki, R., and Watson, C. C., *Ind. Eng. Chem. Proc. Des. Dev.* **5,** 62 (1966).
7. Firth, J. G., and Holland, B. H., *Nature* **217,** 1252 (1968).
8. Firth, J. G., and Holland, H. B., *Trans. Faraday Soc.* **65,** 1121 (1969).

9. Trimm, D. L., and Lam, C. W., *Chem. Eng. Sci.* **35,** 1405 (1980).
10. Yu Yao, Y. F., *Ind. Eng. Chem. Prod. Res. Dev.* **19,** 293 (1980).
11. Cullis, C. F., and Willatt, B. M., *J. Catal.* **83,** 267 (1983).
12. Niwa, M., Awano, K., and Murakami, Y., *Appl. Catal.* **7,** 317 (1983).
13. Hicks, R. F., Young, M. L., Lee, R. G., and Qi, H., *J. Catal.* **122,** 280 (1990).
14. Hicks, R. F., Young, M. L., Lee, R. G., and Qi, H., *J. Catal.* **122,** 295 (1990).
15. Drozdov, V. A., Tsyrulnikov, P. G., Popovskii, V. V., Bulgakov, N. N., Moroz, E. M., and Galeev, T. G., *React. Kinet. Catal. Lett.* **27,** 425 (1983).
16. Hiam, L., Wise, H., and Chaikin, S., *J. Catal.* **9, 10,** 272 (1968).
17. Schwartz, A., Holbrook, L. L., and Wise, H., *J. Catal.* **21,** 199 (1971).
18. Halpern, B., Al-Mutaz, I., and Douyon, L., *J. Appl. Phys.* **52,** 5315 (1981).
19. Volter, J., Lietz, G., Spindler, H., and Lieske, H., *J. Catal.* **104,** 375 (1987).
20. Gangwal, S. K., Mullins, M. E., Spivey, J. J., and Caffrey, P. R., *Appl. Catal.* **36,** 231 (1988).
21. Kemball, C., and Patterson, W. R., *Royal Soc. London Proc., Math. Phys. Sci.* **270,** 219 (1962).
22. Patterson, W. R., and Kemball, C., *J. Catal.* **2,** 465 (1963).
23. Morooka, Y., and Ozaki, A., *J. Catal.* **5,** 116 (1966).
24. Gerberich, H. R., Cant, N. W., and Hall, W. K., *J. Catal.* **16,** 204 (1970).
25. Cant, N. W., and Hall, W. K., *J. Catal.* **16,** 220 (1970).
26. Cant, N. W., and Hall, W. K., *J. Catal.* **22,** 310 (1971).
27. Carballo, L. M., and Wolf, E. E., *J. Catal.* **53,** 366 (1978).
28. Yu Yao, Y. F., *J. Catal.* **87,** 152 (1984).
29. Wu, N. L., and Phillips, J., *J. Phys. Chem.* **89,** 591 (1986).
30. Wu, N. L., and Phillips, J., *J. Catal.* **113,** 383 (1988).
31. Anderson, J. R., "Structure of Metallic Catalysts." Academic Press, New York, 1975.
32. Benson, J. E., and Boudart, M., *J. Catal.* **4,** 704 (1965).
33. Hicks, R. F., Yen, Q. J., and Bell, A. T., *J. Catal.* **89,** 498 (1984).
34. Levenspiel, O., "Chemical Reaction Engineering." Wiley, New York, 1972.
35. McCabe, R. W., Wong, C., and Woo, H. S., *J. Catal.* **114,** 354 (1988).
36. Bayer, G., and Wiedemann, H. G., *Thermochim. Acta* **11,** 79 (1975).
37. Primet, M., *J. Catal.* **88,** 273 (1984).
38. Greenler, R. G., Burch, K. D., Kretzchmar, K., Bradshaw, A. M., and Hayden, B. E., *Surf. Sci.* **152/153,** 338 (1985).
39. Rothschild, W. G., Yao, H. C., and Plummer, H. K., *Langmuir* **2,** 588 (1986).
40. Hayden, B. E., Kretzschmar, K., Bradshaw, A. M., and Greenler, R. G., *Surf. Sci.* **149,** 394 (1985).
41. Yao, H. C., Sieg, M., and Plummer, H. K., *J. Catal.* **59,** 365 (1979).
42. Butt, J. B., and Petersen, E. E., "Activation, Deactivation, and Poisoning of Catalysts," Chap. 3. Academic Press, New York, 1988.
43. Voorhies, A., *Ind. Eng. Chem.* **37,** 318 (1945).
44. Barbier, J., *Appl. Catal.* **23,** 225 (1986).